

Questioning the ASTM G32-16 (stationary specimen) standard cavitation erosion test

Matevž Dular^{a,c,*}, Guillermo Enrique Barragan Montalvo^b, Marko Hočevár^a, Lovrenc Novak^a, Claus Dieter Ohl^c, Martin Petkovsek^a

^a Faculty of Mechanical Engineering, University of Ljubljana, Askerceva 6, 1000 Ljubljana, SI, Slovenia

^b Escuela Politécnica Nacional, Av. Ladrón de Guevara E11-253, Quito 170525, Ecuador

^c Institute for Physics, Otto von Guericke University, Universitätsplatz 2, 39106 Magdeburg, DE, Germany

ARTICLE INFO

Keywords:

Cavitation
Bubble
Erosion
G32 standard

ABSTRACT

Cavitation erosion is one of the most severe problems encountered in hydraulic turbomachinery. When testing the materials, the engineers usually rely on standardized procedures. The most common one being the vibratory ASTM G-32 test, which offers two possibilities of performing the test – the direct, where the specimen is attached to the ultrasonic device and the indirect, where the specimen is stationary and exposed to the ultrasonic horn, positioned just 0.5 mm from it. The erosion rates from the two are significantly different and a question may be asked if they are at all comparable and further on are they comparable to the “real-life” hydrodynamic cavitation which occurs in turbomachinery.

In this study we performed erosion tests on a stationary specimen where the gap between the specimen and the horn was varied from 0.3 to 4 mm. In addition, we used high speed visualization to observe the cavitation in the gap.

We observed that the cavitation erosion rate strongly depends on the gap. From visualization we see that the cavitation dynamics significantly changes in a small gap, leading to a large, but 2-dimensional cavitation bubbles which collapse very slowly, compared to the small spherical ones in a larger gap.

We investigated the probability of shock wave occurrence and derived a very simple model, which gives accurate qualitative predictions of experimental data.

Finally, the study puts into question the validity of ASTM G32 test – the most common approach used in engineering today.

1. Introduction

Cavitation occurs when the pressure of a liquid is locally reduced to pressure below its vapour pressure, resulting in the formation, growth, and collapse of vapor-filled cavities. When it comes to flowing liquid applications, such as turbomachinery, where the working fluid is subjected to abrupt pressure changes, the collapse of cavities leads to undesirable effects such as surface damage, mass loss, decreased performance, and the attraction of vibration and noise [1]. Regarding hydraulic machinery (pumps, turbines, propellers, etc.), cavitation also leads to a periodical decrease in efficiency and its useful life. For decades, cavitation has been a highly researched phenomenon. A lot of effort has also been put into the characterization of cavitation and its effects on exposed surfaces of different materials [2].

Collapse of the cavitation bubble is characterized by the compression of the gasses within it and the subsequent emission of shock waves [3,4,5,6,7]. Additionally, in cases where the collapse occurs near a rigid wall, a micro jet can form from the outermost side of the bubble, directed towards the wall, reaching hundreds [8] and even thousands [9,10] meters per second. Both shock wave emission and jet impingement produced by bubble collapse generate impulsive stresses that exert mechanical loads on solid surfaces, causing plastic deformation, material failure, and progressive mass loss.

Regarding the erosive effects of cavitation, there are two different standard test methods used to compare the cavitation erosion resistance of solid materials: ASTM G32-16 [11] and ASTM G134-17 [12]. In the G134-17 standard, a submerged cavitating jet originating from a nozzle strikes the surface of a test specimen of a specific material [12] while in

* Corresponding author at: Faculty of Mechanical Engineering, University of Ljubljana, Askerceva 6, 1000 Ljubljana, SI, Slovenia.

E-mail address: matevz.dular@fs.uni-lj.si (M. Dular).

the test that follows the G32-16 standard, a magnetostrictive or piezoelectric transducer generates longitudinal ultrasonic oscillations, which are then amplified by a probe (horn) and transmitted to a liquid medium in order to induce cavitation into a threaded button-shaped sample affixed to the end of the horn [11]. A hemispherical cavitation cloud forms and undergoes severe dynamics, resulting in bubble cloud growth and collapse [13,14]. More specifically, in the ASTM G32-16 [11] standard the horn tip – “button” serves as a mounting of a material specimen (Fig. 1A). As it is exposed to cavitation it sustains severe damage in a short period of time. Additionally, the standard offers a different approach for cavitation erosion testing utilizing the same apparatus, known as the “stationary”, “indirect” or “alternative” specimen method (Fig. 1B). Regarding this configuration, the horn tip equipped with a strongly cavitation erosion resistant tip (e.g., titanium) is placed at a small distance (0.5 mm) from the stationary material sample. This arrangement leads to the formation of cavitation clouds between the specimen and the surface of the tip. The vibratory method described in ASTM G32-16 [11] is most widely used in industrial testing of the cavitation-erosion resistance of various materials.

Besides the two mentioned standard tests, cavitation tunnels and rotating disk apparatus are widely used in cavitation erosion research. Cavitation tunnels are variable-pressure water tunnels where cavitation can be induced by different mechanisms (venturi constriction, various geometry wedges, etc.) coupled with a large set of measurement tools [15]. A rotating disk apparatus recreates the real flow conditions of rotating hydraulic machines; in this device, the sample is located on a disk, where cavitation is induced by the relative movement of holes or bolts in the system [16]. Steller [17] implies that while cavitation tunnels and rotating disk tests would provide similar cavitation load conditions to those encountered in hydraulic machinery and fluid flow systems, the higher cost of use and complexity make their usage inefficient in industry.

The usual testing procedure according to the ASTM G32-16 standard begins with an accurate measurement of the initial weight of the specimen, then the sample is placed in the test rig and exposed to cavitation for a selected period of time. This specimen has to be periodically removed from the rig to record its weight and enable the calculation of weight loss as a function of time. Significant parameter values such as the fluid temperature, liquid beaker volume, horn tip submergence beneath the free surface, frequency, and amplitude of the oscillations are all prescribed by the ASTM G32-16 method [11].

According to the G32-16 standard, both stationary and attached specimen methods can be used to test the cavitation-erosion resistance of a specific material. The “stationary specimen method” is widely used among researchers, since the samples are easier to manufacture and handling is faster. However, it is known that the damage caused by the indirect method is significantly smaller compared to the obtained with the direct one – studies [18,19] showed that the ASTM G32-16 “stationary specimen method” erosion rates can be up to three times lower than the ones obtained with the attached specimen method. Additionally, the standard and specifically the stationary sample approach itself

is being repeatably questioned as the conditions in the ultrasonic cavitation do not match the ones in application – namely hydrodynamic cavitation. Several authors [17,20,21,22] emphasize the significance of the relationship between cavitation-erosion and flow velocity when it comes to hydraulic machinery applications. Franc et al. [23] established the influence of the flow velocity on the pitting wear mechanism on material surfaces. Chahine et al. [20] discovered the strong relationship between the increasing rate of supply of cavitation-nuclei (as a result of increase of the flow velocity) and impulsive pressure pulses. Regarding the material response to cavitation, they [20] also proposed that the mismatch between the vibratory apparatus cavitation-erosion test results and the hydrodynamic ones could be related to the material plasticity. While in ultrasonic cavitation the plasticity is predominantly controlled by thermally activated dislocation dynamics, for hydrodynamic cavitation plasticity can be described more by viscous drag mechanisms [2].

Despite the above mentioned differences between the behavior of ultrasonic induced cavitation and hydrodynamic cavitation, vibratory apparatus are widely used in cavitation-erosion resistance tests for hydraulic machinery. Steller [17] used ultrasonic and hydrodynamic approaches to compare erosion rates on different materials, finding similar erosion rates between ASTM-G32 standard test rigs and ASTM-G134 and rotating disk ones. On the other hand, they also noted discrepancies between these different test methods when quantitative analyses were performed.

In order to determine if the erosion rates obtained with the application of ASTM G32-16 methods are comparable to those on hydraulic machinery and fluid flow systems, it's necessary to have a proper understanding of the cavitation dynamics and its behavior due to the gap distance changes between the cavitation source and the specimen. There were several attempts to do this before. For example, Brunton et al. [24] and Endo et al. [25], Kikuchi and Hammitt [26] searched for the optimum gap distance, Dursun et al. [27] investigated the shape of the cavitation cone and its erosiveness at various (larger) gaps. Hansson and Morch approached the problem theoretically, comparing the hemispherical and cylindrical collapses [28]. One of the recent studies by Schreiner et al. [29] approach the explanation of the erosion vs. gap trend from a numerical perspective. They correlate the aggressiveness to the harmonic and subharmonic collapse events within the gap. This was also studied by Priyadarshi et al. [30] who specifically focused to bulk temperature influence on the development of pressure fields inside the gap.

In the present study, the influence of the distance between the ultrasonic horn tip and the specimen has been investigated. Both erosion tests and visualization of cavitation dynamics were performed to elucidate the physics behind them. To do this we rely mainly on high speed observation, focusing also to the dynamics of shockwaves.

2. Experimental set-up

Experiments were performed at the Department for Power

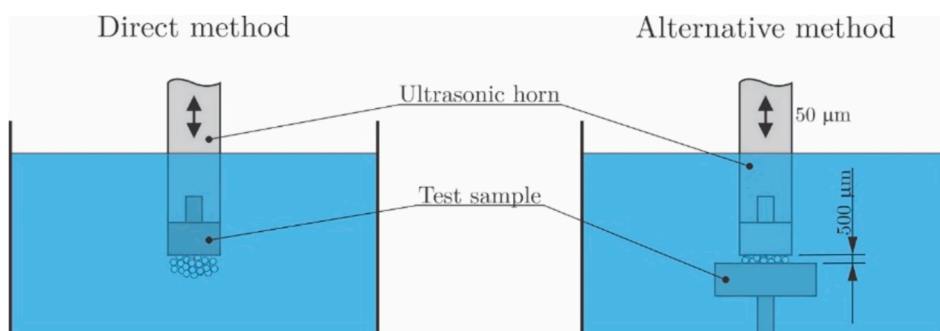


Fig. 1. According to ASTM G32 standard one can use stationary (left) or attached specimen (right). Damage of the two is significantly different.

Engineering, Faculty of Mechanical Engineering, University of Ljubljana, Slovenia and at Institute for Physics, Otto von Guericke University, Magdeburg, Germany.

2.1. Set up

Cavitation-erosion tests were performed according to the alternative ASTM G32-16 “stationary specimen” method, apart from the diameter of the horn – the tip threatened to the end of the probe was made out of Ti-6Al-4V titanium alloy, with 12.7 mm in diameter. The current set up (Fig. 2) utilized a commercially obtained 20-kHz ultrasonic transducer Cole-Parmer 750 W as source of cavitation, to which is attached a suitably designed ultrasonic probe. The peak-to-peak amplitude of the tip followed recommendation in the standard [11] and was 50 μm . A linear translation stage with a reading accuracy of 10 μm (STANDA 7T175-150) allowed precise control of the distance between the surface of the specimen and the horn tip. Cavitation was visualized and mass loss was measured for gap distances ranging from 0.3 mm to 5 mm. The arrangement was immersed 10 \pm 2 mm in a vessel filled with water. The arrangement was immersed 10 \pm 2 mm in a vessel filled with water. The vessel size was 150 \times 150 \times 100 mm (width, length, depth). A cooling coil (not shown in Fig. 2) has been located around the ultrasonic probe in order to maintain a temperature of 25 \pm 2 $^{\circ}\text{C}$. During the long term operation, the ultrasonic horn itself needs to be cooled to maintain its efficiency. This was achieved by an internal air-cooling system (not shown in Fig. 2).

2.2. Erosion

Erosion was evaluated on an aluminium square-shaped specimen with dimensions of 30x30x10 mm. According to the ASTM G32-16 method, the test samples have been weighed accurately before the testing began. A precision scale Sartorius MC 210 S with resolution of 0.01 mg was used. Each specimen has been obtained from a pure Al surface-polished plate using a water jet cutter, which guarantees the fitting of the sample on the above-mentioned set up. The total time of sonication for each test was 120 min, divided into weighting lapses of 15 min in order to obtain a history of mass loss versus time. During the testing the temperature of the medium was recorded by a thermocouple. The weighting process consisted of a careful extraction of the specimen in order to prevent any kind of damage on the surface, then the specimen was dried at ambient temperature for 5 min and weighted. Each test (gap) was repeated 5 times.

2.3. Visualization

To study the cavitation dynamics inside the gap between the horn and the wall a high-speed camera was used. Shimadzu Hyper Vision HPV-2 high speed video camera recorded at a framerate of 500,000 fps. The image resolution was 312x260 pixels. A mirror was used to gain visual access to the frontal view of the cavitation inside the gap.

Two types of illumination were used (left in Fig. 2). Firstly, for the “conventional” visualization of cavitation in the gap a frontal light was used. Secondly, to observe shockwaves, which are emitted at cavitation cloud collapse a mode-locked fiber-based femtosecond laser (EXPLA FemtoLux 3, 515 nm wavelength) was used for backlight illumination. Approximately 200 fs long laser pulses were synchronized with the image acquisition such that a single laser pulse illuminated each frame. This technique allowed us to avoid all motion blurring and enabled the imaging of the shock waves.

3. Results

3.1. Erosion

The cumulative mass loss curves for the specimens at different gap sizes are shown in Fig. 3.

The samples tested at a distance of 1 mm showed a cumulative mass

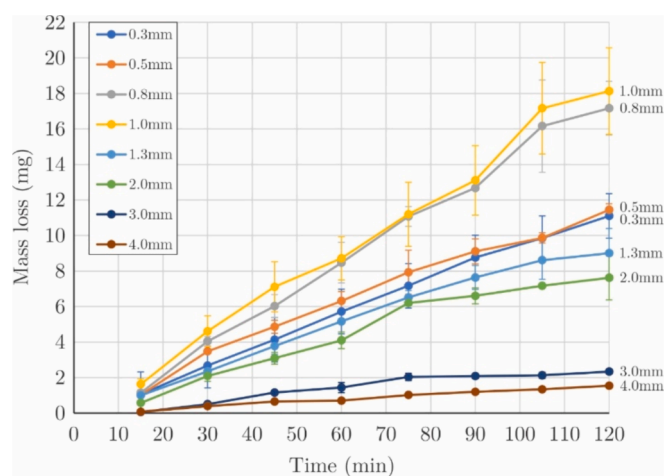


Fig. 3. Cumulative mass loss curves for the specimens at different gap sizes.

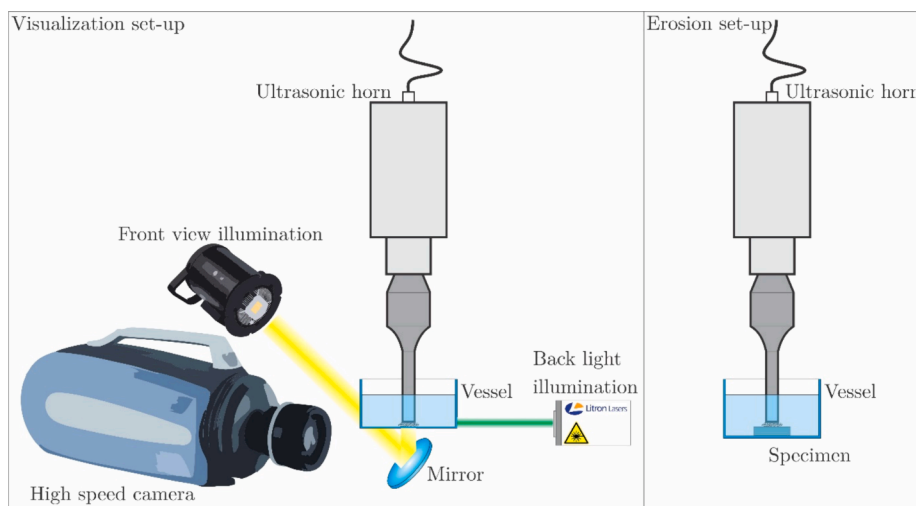


Fig. 2. Experimental set-up for cavitation, shock wave and damage evaluation.

loss of roughly 18 mg at 120 min, at 0.8 mm of gap the cumulative mass loss was ~ 16 mg. Tests performed at a distance of 0.5 mm (which is the standardized distance using the ASTM G32-16 stationary specimen method) reached a value of approximately 9 mg. Further on, for gap distances at 0.3, 1.3 and 2.0 mm the mass loss was still lower. Mass losses for the largest gap distances (3 and 4 mm) are marginal – of the order of 2 mg after 120 min of exposure to cavitation.

Fig. 4 depicts the macroscopic morphologies of each tested gap distance at 120 min of cavitation.

A reduction of the eroded area as the gap between the tip of the probe and the sample increases can be observed. This is related to the cone-like cavitation structure formation – typical of vibratory test methods. At a distance of 1 mm erosion damage is equally distributed over the surface. For gaps of 1.3 mm and 2 mm an erosion ring is formed between the center of the cavitated area and its edge. The formation of the bubbly ring at these distances is according to [31] a result of the vibration mode of the radiation surface, which determines the spatial distribution of bubble-rich ring region. Another reasoning for its formation, but more focused on the position of the ring, based on fluid mechanics and analytical mechanics, can be found in [32]. For samples tested at distances of 3 mm and 4 mm the edges of the eroded area are diffuse and small pits can be observed erratically distributed over the surface.

The average mass loss rates for each of the distances tested with the ASTM G32-16 indirect method are shown in Fig. 5.

The maximum mass loss rate of 0.15 mg/min was obtained with a 1 mm gap between the sonotrode tip and the sample, which agrees with previous studies [26]. For both distances greater and smaller than 1 mm, a decrease of the mass loss rate can be observed. A very obvious peak at 1 mm with rapid decrease for both smaller and larger gaps implies that the erosion is likely closely linked to the dynamics of cavitation inside the gap. The results of observations are presented in the next section.

3.2. Cavitation dynamics

Fig. 6 depicts the cavitation dynamics at different gap distances between the ultrasonic horn and a solid stationary specimen. The image sequences were captured through a solid transparent sample (see Fig. 2, left). One can notice a dark ring across the surface of the tip (at about 70 % of the radius) – this is a result of wear from past use. In the present experimental campaign, the horn operated at high enough amplitude to achieve intensive cavitation far from incipient stage, where the defects could act as generators of cavitation nuclei and where these could

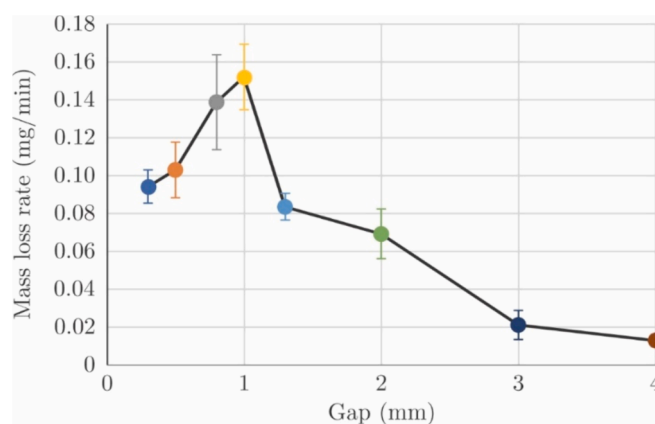


Fig. 5. Average mass loss rates for different tested distances.

influence cloud dynamics. Hence, the presence of wear is not relevant for the present study.

One can immediately notice the difference in the cavitation topology (please see video material in the supplementary for better representation). As the gap distance between the specimen and the tip of the horn increases, cavitation changes from a single large and thin (squeezed) cloud to multiple more spherical cavitation clouds. From the general appearance of cavitation we see that a topological transition occurs roughly at 1 mm gap distance. The change in the appearance in the images can be explained by the reflection of the incoming light on the surface of the bubbles. When they are squeezed, the light passes them perpendicularly and is reflected back to the camera at the tip of the horn, hence the area appears transparent (or bright), when they are spherical, they reflect the light in all directions, hence they appear darker.

Fig. 7 shows a scheme that summarizes the dynamics of the bubbles for distances below 1 mm and those above 1 mm.

For a small gap the cavity is squeezed between the surfaces and oscillates slowly. The collapse begins from two sides (facing each other) of the tip. As the jets meet in the middle they progress to collapse the remaining vapour pocket. In the meantime the vapour pocket begins to form again following the inwards rushing jet.

For the cases with the larger gaps size, multiple cavitation clouds appear and collapse almost independently from each other, likely causing erosion simultaneously at multiple sites in the process. Another

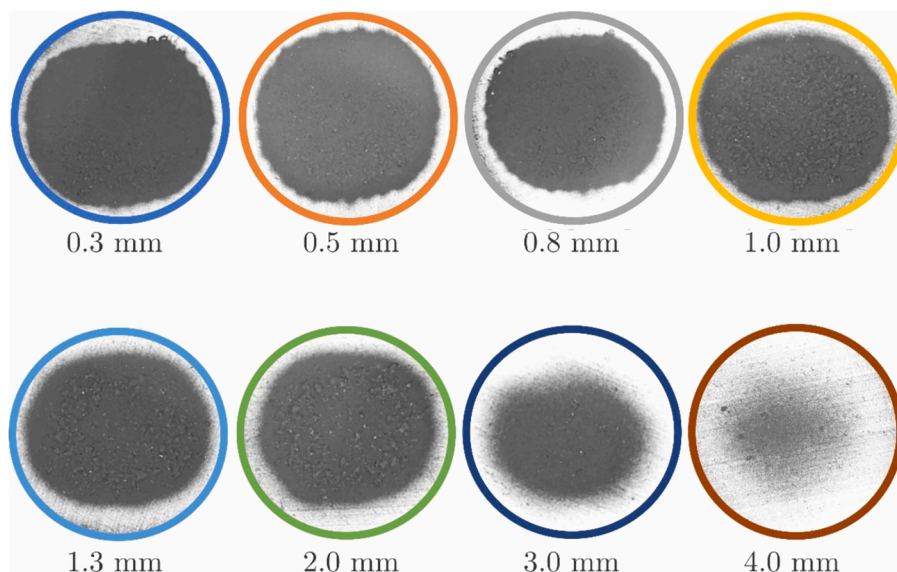


Fig. 4. Macroscopic morphologies of different tested distances at 120 min.

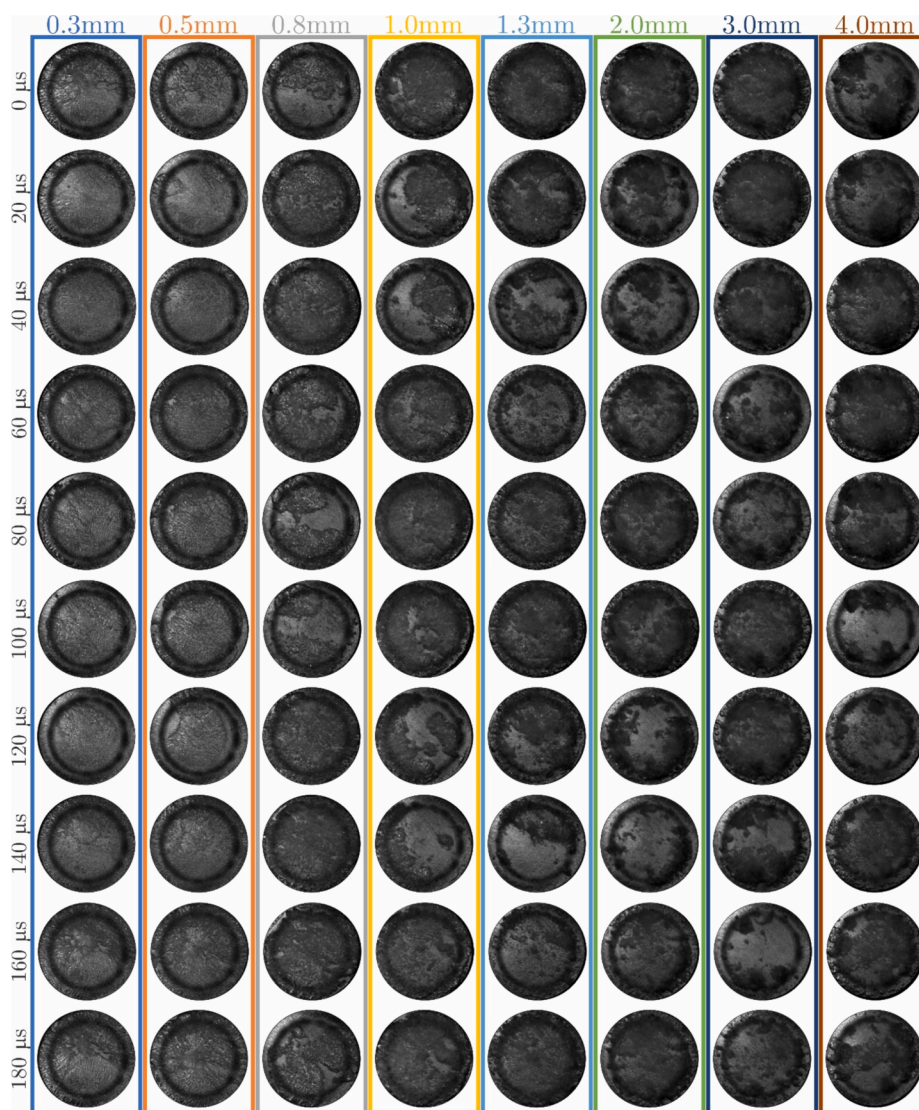


Fig. 6. Cavitation dynamics at different gap sizes (see video material in supplementary).

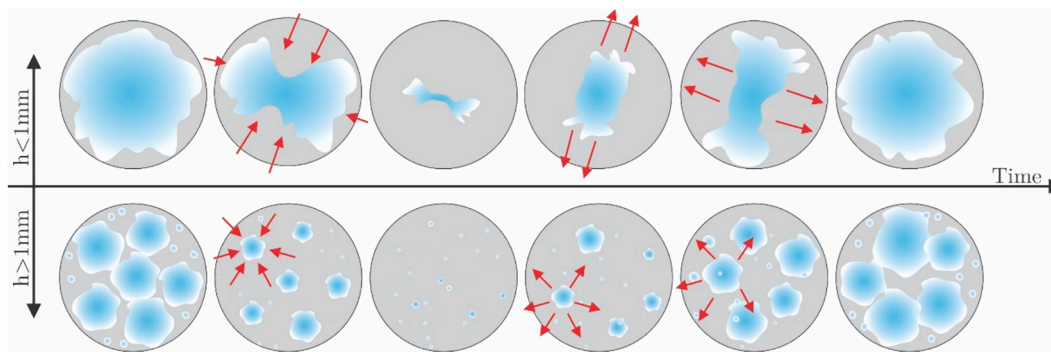


Fig. 7. Schematics of the dynamics of the bubble(s) as a function of the gap size.

reason for the more severe erosion likely also lies in the lesser shielding of the shock wave since the gap is not fully populated by bubbles [33].

Observations presented here are in line with previous detailed studies of spatial distribution of cavitation bubbles in thin liquid layers on ultrasonic horn with much larger diameter [34,35]. As in the present experiment they found that the cavitation appearance changes significantly when the gap is altered – from “disc shaped structures” (squeezed

bubbles in the present paper) in small gaps to what they refer as “smokers” (clouds in the present paper) in larger gaps.

3.3. Shock wave dynamics

Cavity collapse causes the emission of shockwaves through the fluid. In Fig. 8, examples of detected shockwaves at various gaps

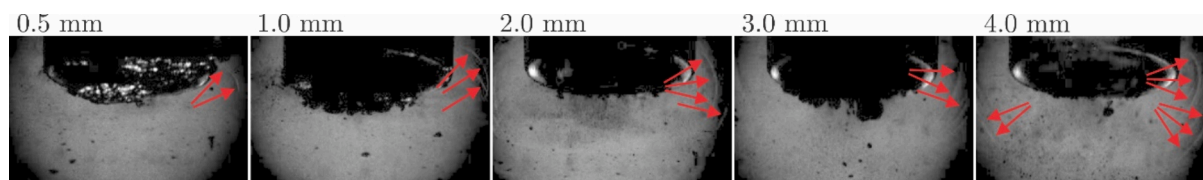


Fig. 8. Typical shock wave detection at different gap sizes. See video material in supplementary.

between the tip of the sonotrode and the solid surface are shown.

Fig. 8 only serves as an illustrative narrative. For small gap distances the bubble is squeezed between the surfaces (see also Fig. 6 and movies in the supplementary). Examples of shock waves can be seen. For the case of a 0.5 mm gap one was rarely observed. Small probability of shock wave emission can be linked to the slower dynamics of the cavity in the small gap. Also, reduced number of shockwaves can be a result of the “shielding effect” of the bubble cloud – tightly packed vapor region in the thin gap between the horn tip and the surface attenuates the propagation of the pressure wave into the fluid [33]. On the other hand, at larger gaps, shock waves were more probable and also multiple and simultaneous during one single period of horn oscillation. This can be linked to the observation of a number of cavitation clouds (clusters consisting of multiple bubbles) that upon collapse each emit a shockwave.

The results of a study statistically quantifying the occurrence of shockwaves are shown in Fig. 9. First a relatively long series of images was recorded (~7000 at 100,000 fps), then throughout the series two successive images were compared to reveal the presence of a shock wave. The magnitude and the clearness of the shock waves of course varies through time – some are evenly powerful; some are hardly seen. To detect them we used a certain threshold. This could of course mean that some of the weaker shocks would go unnoticed, but these are also less likely to cause significant damage. The number of detected shock waves was compared to the number of horn oscillations and finally the probability (in percentage) was determined as the number of detected shockwaves divided by the number of ultrasonic horn oscillations.

Due to a simplistic approach to detection of the shockwaves, the value of the data in Fig. 9 is mainly qualitative – it represents well the change of cavitation intensity as the gap size is altered. We see that the shock wave occurrence exhibits a linear increase with the increase of the gap distance.

The shock wave emission can be directly correlated with the cavitation cloud collapse [3,7,36]. The maximum shockwave occurrence probability of approximately 15 % was recorded at a 4 mm gap distance

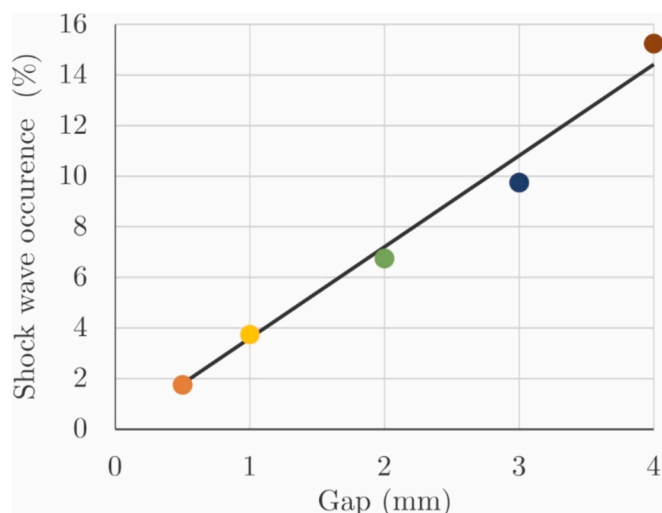


Fig. 9. Shock wave occurrence rate as a function of the gap size.

between the tip of the sonotrode and the surface of the specimen. At this distance the gap seems not play a significant role anymore and the cavitation dynamics begins to resemble the one of unbounded horn tip and it was show by Znidarcic et al. [37,38] that the developed cavitation cloud oscillation follows about 1/7th to 1/5th (14 to 20 %) of the horn oscillation. The extended life of a cavitation cloud can be attributed to the inertia of the host liquid preventing bubble structures that inflate to a sufficient size during a tension phase. This results in cavitation cloud going over several non-collapsing deflations between each collapse cycle [39]. By reducing the gap, the (now squeezed) cavitation cloud covers the whole surface of the tip and even harder follows the driving frequency (the collapse time is longer than the period of oscillation). Hence the shockwave becomes even less likely and drops to only about 1/50th (2 %) of the horn oscillation.

3.4. Results on single bubble collapse in a thin gap

A possible way to interpret the results obtained in the ultrasonic horn experiments is the observation of single bubble dynamics in a thin liquid gap and its comparison to the dynamics of an unbounded bubble. Additional tests were performed, where we induced single cavitation bubbles by laser light breakdown.

The setup is essentially the same as the one used in [40] or [41]. The growth and collapse of a spherical (unbounded) bubble is shown in Fig. 10.

At $t = 0.5 \mu\text{s}$ one can see a shockwave (the large circle (with 0.75 mm radius)) generated by the plasma breakdown. The shock wave traveled approximately 0.75 mm in 0.5 μs , which corresponds well to the sonic velocity in water (1500 m/s). At plasma breakdown a spherical bubble is formed (smaller dark circle in the second image). The growth phase of the bubble continues until $t = 55 \mu\text{s}$, when the bubble reaches its maximum radius – 0.74 mm. As there are no boundaries in the vicinity, the bubble begins to collapse spherically. It collapses at $t = 108 \mu\text{s}$, when one can see a bright spot indicating luminescence from hot compressed gases. The bubble then undergoes several rebounds. One can notice small stationary circles in the image – these are droplets on the outside of the container which were unfortunately noticed after the experiment (they of course do not influence the dynamics of the bubble).

Fig. 11 shows the growth and collapse of a cylindrically shaped bubble. A bubble of a similar volume was created in a thin gap between two glass plates. The gap size was 0.24 mm, which is again close to the smallest gap investigated in the ultrasonic horn setup (also considering the movement of the horn). The dynamics is shown in Fig. 11.

As in Fig. 10, also in Fig. 11, both the bubble (small circle) and the shock wave front (larger less defined circle) can be seen.

The shock wave is just one of multiple traveling at different velocities due to the interplay of sound speeds in the water and the glass plates that are squeezing the bubble. One can also notice that the shock is less pronounced than in the case of spherical bubble. This is likely due to the presence of many small cavities which form due to the momentary pressure drop during the transition of the Lamb wave – an elastic wave that propagates at very high velocity (>3000 m/s) through the upper and lower glass plate with the amplitude perpendicular to the plate (see [42]). The occurrence of the Lamb wave is specific to this particular experiment (Fig. 11) and is not encountered in the ultrasonic horn tests. The difference in the appearance between the bubble in Figs. 10 and 11

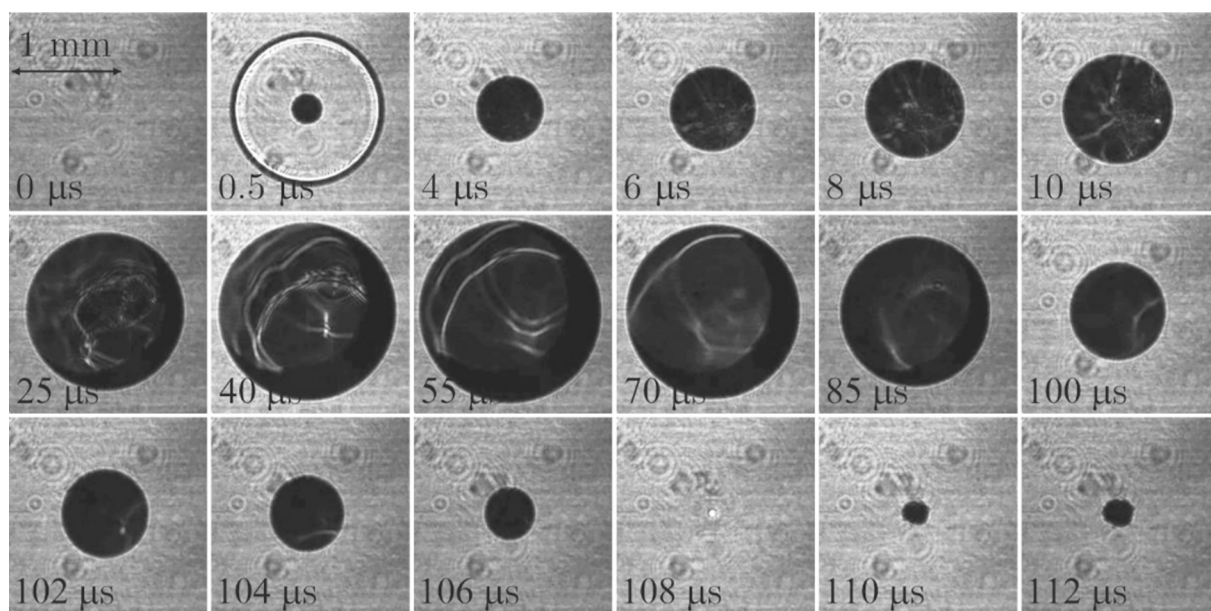


Fig. 10. Unbounded spherical bubble growth and collapse ($R_{\max} = 0.74 \text{ mm}$, $V_{\max} = 1.70 \text{ mm}^3$). See video material in supplementary.

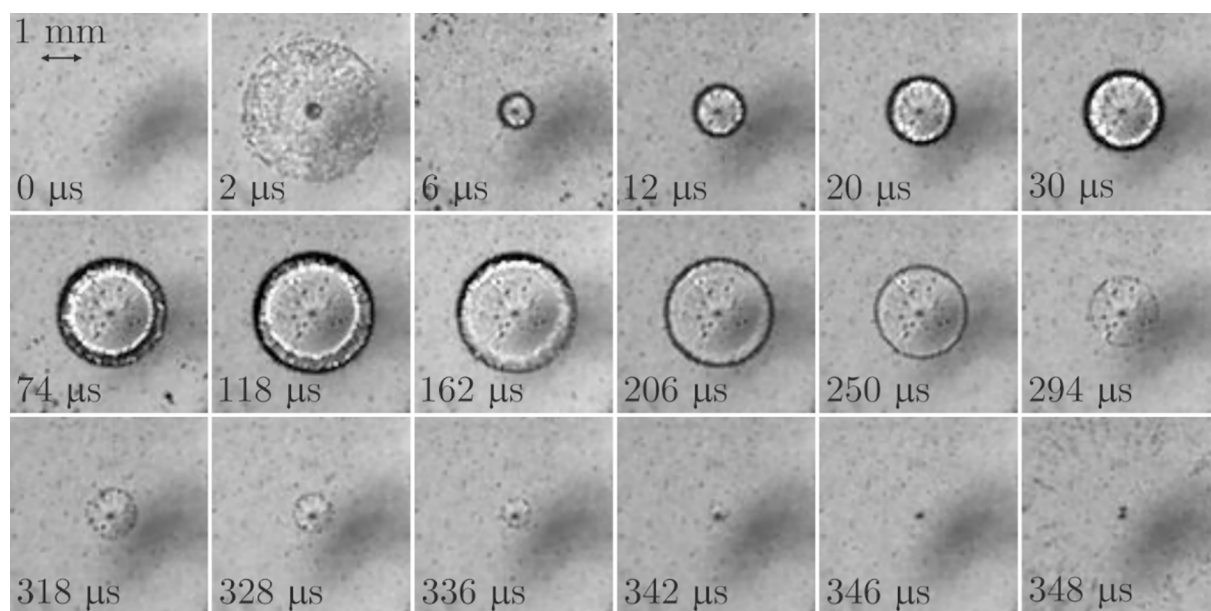


Fig. 11. Cylindrical bubble growth and collapse ($h = 0.24 \text{ mm}$, $R_{\max} = 1.49 \text{ mm}$, $V_{\max} = 1.67 \text{ mm}^3$). See video material in supplementary.

is a result of their shape. In Fig. 10 it is spherical, hence the back light is reflected on its surface, and it does not reach the camera – the bubble appears dark. The bubble in Fig. 11 is squeezed between the plates. Since it is cylindrical, the light passes through it on top and bottom (the surfaces are perpendicular to the illumination and the camera), but not at the circumference, which in this case appears black. The growth is much slower – the bubble reaches its maximum size (radius of 1.49 mm) at $t = 162 \mu\text{s}$. Following this, the bubble collapses symmetrically (cylindrically) and the minimum size is reached at about $t = 342 \mu\text{s}$. In the final image of the sequence at $t = 348 \mu\text{s}$ one can again observe very small bubbles scattered in radial direction from the point of the main bubble collapse – this is again a result of the Lamb wave that progressed at a very high velocity through the glass plates and creating a momentary low pressure region in its wake [42].

Obviously, the collapse of a cylindrical bubble is much slower and consequently less aggressive. This is nicely shown in Fig. 12 which

depicts the nondimensionalized (to the maximal radius of each bubble and to the spherical bubble collapse time) bubble radii vs. time for the cases in Figs. 10 and 11.

The growth rate of the cylindrical bubble first surpasses the spherical one. This is the result of the Lamb wave which forms due to the minute deformation of the two plates. The rate then slows down and as expected the spherical bubble reaches its maximum radius before the cylindrically shaped one. The collapse of the cylindrical bubble is much slower – compared to the spherical case it takes more than twice the time for it to collapse completely. This is consistent with the observations and simulations for even thinner (nanometric) gaps [42]. At the collapse of the bubble a shock wave is generated, which at its origin, also triggers the Lamb wave in the plates (see video material in the supplementary). As mentioned before, the Lamb wave, in its wake causes slight depressurization which, in the present experiment, results in a larger rebound of the cylindrical bubble.

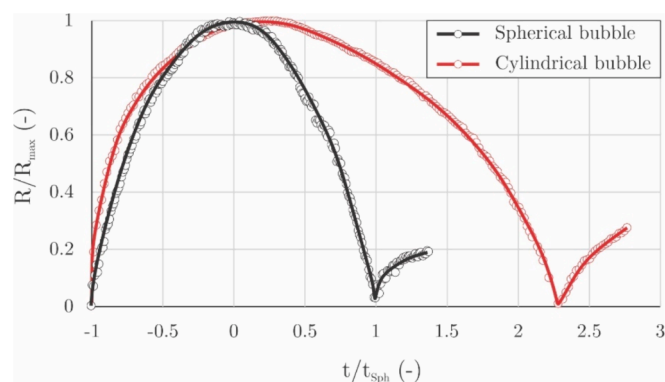


Fig. 12. Time evolution of nondimensional bubble radius for spherical and cylindrical bubble of comparable maximal volume.

Although the presence of the Lamb wave obviously accelerated the growth dynamics of the bubble, the collapse is unaffected by it as it is not present at that time (it is again emitted at the moment of collapse).

4. Discussion

To explain the dependency of cavitation aggressiveness on the gap size (Fig. 5) one can develop a simple algebraic model. Although, cavitation and cavitation erosion are extremely complex phenomena that include shock waves, microjets, high temperatures, fluid structure interaction, material response etc. There were past attempts to include many of them, including use of high-fidelity computational approaches [29,43]. Here we take a different approach, although less elaborate, it

provides valuable insight into the physics of the phenomenon. We show that to qualitatively explain the present experiment, there are only three parameters that one needs to consider. These are i) the probability that a shock wave will occur, ii) the amplitude of the shock wave and iii) the attenuation of the shock wave. The multiplication of the 3 gives a qualitative estimation of the aggressiveness. Also, since we are considering only qualitative comparison, we can nondimensionalize the 3 parameters.

The probability of the shock wave occurrence is given by the measurements shown in Fig. 9. There we see that it increases linearly. However, one can expect it to flatten out as we approach completely unbounded tip of the horn. At this distance the gap will not play a significant role anymore and the cavitation dynamics begins to resemble the one of unbounded horn. As it was shown before [37,38] the developed cavitation cloud oscillation follows about 1/7th to 1/5th (14 to 20 %) of the horn oscillation, leading to the same rate of shock wave emission (when one accepts that the cloud collapse and shock wave emission are directly related [3,7,36]). The idealized and nondimensionalized trend (Eqn. (1) is shown in Fig. 13A.

To measure the shock wave amplitude in constrained geometries, such as the present one, the conventional measurements using hydrophones [36] are not feasible due to bandwidth and geometric constraints. Here, shock wave amplitude can be most accurately assessed by measuring shock front velocity as shown by [44]. This would require highly resolved imaging, which relies on innovative illumination techniques. Since we are not pursuing the accurate measurement here, but are only interested in the general trend, we can focus our attention to the collapse velocity (Figs. 10 to 12). Considering the Rayleigh collapse time and that the pressure inside the bubble changes adiabatically, it can be shown that the maximal pressure will increase with collapse velocity

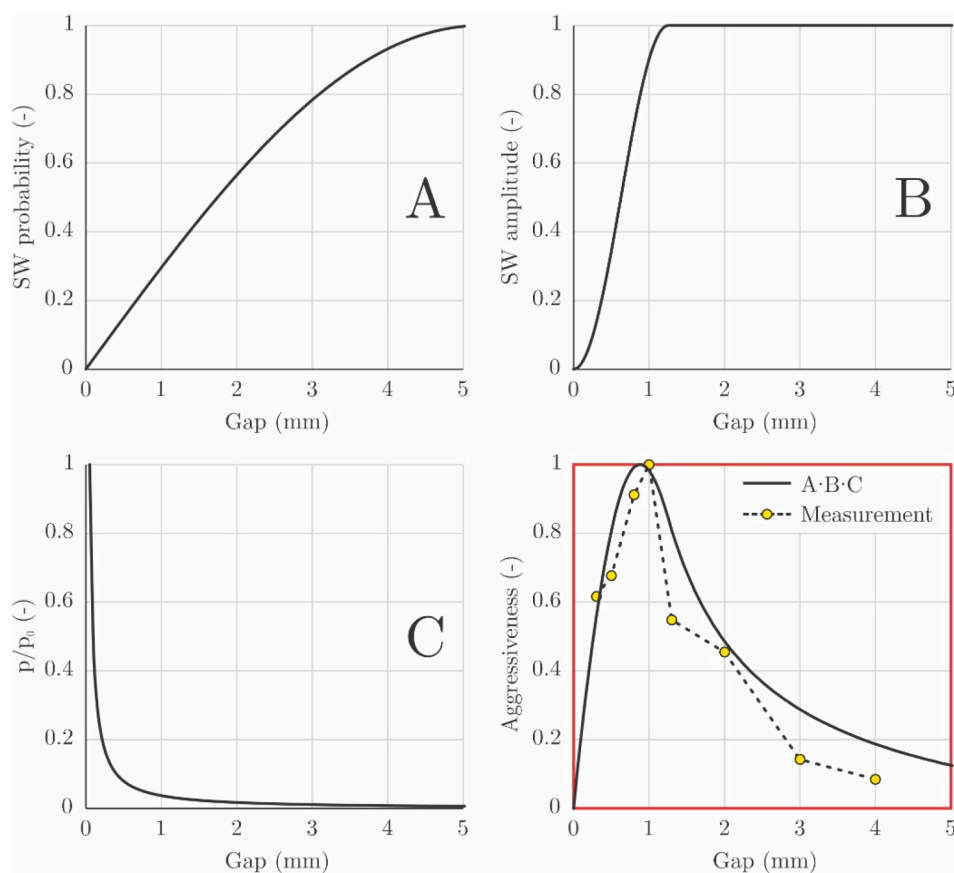


Fig. 13. A very simple model which relates the probability of the shock wave (A), the amplitude of the shock wave (B) and the shock wave attenuation (C). Multiplication of these 3 variables (A·B·C) gives an qualitative estimation of cavitation erosion rate (red square, bottom, right). (For interpretation of the references to colour in this figure legend, the reader is referred to the web version of this article.)

squared [1]. An unbounded bubble (at large gap) will generally have the same collapse velocity. A confined bubble collapses much slower (Figs. 10 to 12). The change from fast to slow collapse will occur when the bubbles transition from spherical to cylindrical shape. The change will be abrupt, and the point of the transition is of course related to the bubbles size. In reality the bubble size is normally distributed over a larger spectrum of radii, with an average value equal to the resonance radius of the bubble. According to Brennen [45], considering that the ultrasonic horn frequency was 20 kHz one can estimate the resonant radius of the bubble R_{res} of about 0.16 mm. It was reported by Quinto-Su et al. [46] that the bubble dynamics approaches that of a spherical bubble as the height of the gap is increased; for $Gap/R_{max} > 7$, the collapse is as fast as in the unconstrained case. The gap size value, where one should not see the influence of the walls for the present setup is 1.1 mm, at which point we flatten out the idealized curve (Eqn. (2) of shock wave amplitude (Fig. 13B).

Finally, the amplitude of the shock wave is attenuated by the distance, hence the damage sustained will be larger when the bubble collapses closer to the wall. The dependency well know from acoustical theory – the amplitude declines exponentially. It was recently studied in detail for the specific case of ultrasonic cavitation by Khavari et al. [33] and their model (Eqn. (3) was adopted here (Fig. 13C).

The models for the variables used in the present discussion and shown in Fig. 13 are given by Eqns. (1), 2 and 3. All are normalized to span from 0 to 1. It is again important to emphasize that they are not meant to be taken as quantitative assessments of the parameters – they are only useful to predict qualitative trends of the variables in question.

$$SW_{probability} = A = \begin{cases} \sin(0.3 \bullet gap); gap \leq 5mm \\ 1; gap > 5mm \end{cases} \quad (1)$$

$$SW_{amplitude} = B = \begin{cases} 0.5 \bullet (1 - \cos(2.5 \bullet gap)); gap \leq 1.1mm \\ 1; gap > 1.1mm \end{cases} \quad (2)$$

$$\frac{p}{p_0} = C = \frac{(2.29 \bullet gap^{-1.1})}{\max(2.29 \bullet gap^{-1.1})} \quad (3)$$

Multiplication of the three parameters, i.e. *Aggressiveness* = $A \cdot B \cdot C$, gives a rough and qualitative estimation of the aggressiveness of cavitation, by the specimen (Fig. 13, red square bottom right).

We see that even a very simple model nicely predicts the trend, which was determined experimentally. Most of the experimental data lies below the model curve, but one needs to bear in mind that we are using the simplest possible model to qualitatively predict the results of a relatively complex experiment. Also, we omitted the use of any factors to make the approach as clean as possible. The maximum damage occurs at roughly 1 mm gap, which is a result of optimal conditions: bubbles already featuring spherical dynamics, enough space for the shock wave formation and small enough distance so that bubbles implode close to the surface of the specimen.

5. Conclusions

The paper discusses observations of the damage sustained by the stationary specimen under and ultrasonic horn. The standard prescribes the gap distance to be 0.5 mm. In our investigation we investigated the influence of varying this distance. It was found that when it is smaller than 1 mm the bubbles occupy cylindrical shape, consequently their collapse is less aggressive. Also, the probability of the shock wave (the trigger for the damage) is smaller.

Single bubble experiments were performed to investigate the dynamics of bubbles in thin gaps. Based on this a very simple reasoning was established, which included only 3 parameters – the shock wave occurrence probability, the amplitude of the emitted shock wave and the attenuation of the shock wave. Multiplication of the three, leads to a very good qualitative prediction of the measured data.

Finally, one needs to mention that at the gap distance of 0.5 mm we are dealing primarily with cylindrical, or at least extremely flattened, bubbles. These cannot be found in “real” applications, such as water turbines, pumps and ship propellers. The evaluation of the materials resistance to cavitation erosion according to the ASTM G32-16 standard (stationary specimen) is therefore questionable and one should at least consider increasing the gap to at least 1 mm to achieve more spherical bubbles.

CRedit authorship contribution statement

Matevž Dular: Writing – original draft, Visualization, Supervision, Methodology, Investigation, Funding acquisition, Formal analysis, Data curation, Conceptualization. **Guillermo Enrique Barragan Montalvo:** Writing – original draft, Investigation. **Marko Hočevar:** Writing – original draft, Methodology. **Lovrenc Novak:** Writing – original draft, Visualization, Methodology. **Claus Dieter Ohl:** Writing – original draft, Methodology, Investigation, Funding acquisition. **Martin Petkovšek:** Writing – original draft, Methodology, Investigation, Data curation, Conceptualization.

Declaration of competing interest

The authors declare the following financial interests/personal relationships which may be considered as potential competing interests: Matevž Dular reports financial support was provided by European Research Council. Matevž Dular reports financial support was provided by Alexander von Humboldt Foundation. Matevž Dular, Martin Petkovšek, Marko Hočevar, Lovrenc Novak reports financial support was provided by Slovenian research and innovation agency. If there are other authors, they declare that they have no known competing financial interests or personal relationships that could have appeared to influence the work reported in this paper.

Acknowledgments

The authors acknowledge the financial support from the European Research Council (ERC) under the European Union’s Framework Program for research and innovation, Horizon 2020 (grant agreement n 771567 – CABUM), the Slovenian Research Agency (Core funding No. P2-0422) and the support from the Humboldt Foundation Friedrich Wilhelm Bessel Research Award.

Appendix A. Supplementary data

Supplementary data to this article can be found online at <https://doi.org/10.1016/j.ultsonch.2024.106930>.

References

- [1] J. P. Franc and J. M. Michel, *Fundamentals of Cavitation*, no. 1. Dordrecht: Kluwer, 2004. 10.1007/s13398-014-0173-7-2.
- [2] Fluid Mechanics and Its Applications vol. 106 (2014), <https://doi.org/10.1007/978-94-017-8539-6>.
- [3] C.E. Brennen, G. Reisman, Y.C. Wang, *Shock Waves in Cloud Cavitation*, in: *Proceedings of the TwentyFirst Symposium on Naval Hydrodynamics, 1992*, pp. 756–771.
- [4] W. Lauterborn, T. Kurz, C. Schenke, C. Ohl, R. Geisler, O. Lindau, Shock waves from cavitation bubbles, *J. Acoust. Soc. Am.* 105 (2) (Feb. 1999) 1232, <https://doi.org/10.1121/1.425927>.
- [5] O. Supponen, D. Obreschkow, P. Kobel, M. Tinguely, N. Dorsaz, M. Farhat, Shock waves from nonspherical cavitation bubbles, *Phys. Rev. Fluids* 2 (9) (Sep. 2017) 093601, <https://doi.org/10.1103/PhysRevFluids.2.093601>.
- [6] Z. Lokar, D. Horvat, J. Petelin, R. Petkovšek, Ultrafast measurement of laser-induced shock waves, *Photoacoustics* 30 (Apr. 2023), <https://doi.org/10.1016/J.PACS.2023.100465>.
- [7] M. Petkovšek, M. Hočevar, M. Dular, Visualization and measurements of shock waves in cavitating flow, *Exp. Therm Fluid Sci.* 119 (Nov. 2020) 110215, <https://doi.org/10.1016/J.EXPTHERMFLUSCI.2020.110215>.

- [8] M. Dular, T. Pozar, J. Zevnik, R. Petkovšek, High speed observation of damage created by a collapse of a single cavitation bubble, *Wear* 419 (Jan) (2019) 13–23, <https://doi.org/10.1016/j.wear.2018.11.004>.
- [9] F. Reuter, C.D. Ohl, Supersonic needle-jet generation with single cavitation bubbles, *Appl. Phys. Lett.* 118 (13) (Apr. 2021) 134103, <https://doi.org/10.1063/5.0045705>.
- [10] C. Lechner, W. Lauterborn, M. Koch, R. Mettin, Fast, thin jets from bubbles expanding and collapsing in extreme vicinity to a solid boundary: A numerical study, *Phys. Rev. Fluids* 4 (2) (Feb. 2019) 021601, <https://doi.org/10.1103/PHYSREVFLUIDS.4.021601/FIGURES/5/MEDIUM>.
- [11] ASTM G32-16, "Standard Test Method for Cavitation Erosion Using Vibratory Apparatus," *ASTM International, West Conshohocken, PA, 2016*, www.astm.org, 2016.
- [12] ASTM G134 : Standard Test Method for Erosion of Solid Materials by Cavitating Liquid Jet. Accessed: Jan. 03, 2023. [Online]. Available: https://global.ihs.com/doc_detail.cfm?document_name=ASTM%20G134&item_s_key=00234644.
- [13] A. Žnidarčič, R. Mettin, C. Cairós, M. Dular, Attached cavitation at a small diameter ultrasonic horn tip, *Phys. Fluids* 26 (2) (2014) pp, <https://doi.org/10.1063/1.4866270>.
- [14] G. Kozmus, J. Zevnik, M. Hočevar, M. Dular, M. Petkovšek, Characterization of cavitation under ultrasonic horn tip-Proposition of an acoustic cavitation parameter, *Ultrason. Sonochem.* 89 (2022) 106159, <https://doi.org/10.1016/j.ultrasonch.2022.106159>.
- [15] A.K. Krella, D.E. Zakrzewska, Cavitation Erosion – Phenomenon and Test Rigs, *Adv. Mater. Sci.* 18 (2) (Jun. 2018) 15–26, <https://doi.org/10.1515/ADMS-2017-0028>.
- [16] A. Osterman, B. Bachert, B. Sirok, M. Dular, Time dependant measurements of cavitation damage, *Wear* 266 (9–10) (Apr. 2009) 945–951, <https://doi.org/10.1016/J.WEAR.2008.12.002>.
- [17] J. Steller, International Cavitation Erosion Test and quantitative assessment of material resistance to cavitation, *Wear* 233–235 (Dec. 1999) 51–64, [https://doi.org/10.1016/S0043-1648\(99\)00195-7](https://doi.org/10.1016/S0043-1648(99)00195-7).
- [18] Jonty Mago, Sandeep Bansal, Dheeraj Gupta, and Vivek Jain, "Investigation of Erosion and Pressure for Direct and Indirect Acoustic Cavitation Testing," in *International Conference on Trends in Science, Engineering and Management (ICTSEM-2019)*, 2019. Accessed: Dec. 14, 2023. [Online]. Available: https://www.researchgate.net/publication/339385461_Investigation_of_Erosion_and_Pressure_for_Direct_and_Indirect_Acoustic_Cavitation_Testing.
- [19] V. Cojocar, V. Constantin Campian, D. Frunzaverde, A comparative analysis of the methods used for testing the cavitation erosion resistance on the vibratory devices, *U.P.B. Sci. Bull., Series D* 77 (4) (2015) pp.
- [20] G.L. Chahine, J.P. Franc, A. Karimi, Mass loss and advanced periods of erosion, *Fluid Mech. Appl.* 106 (2014) 97–121, https://doi.org/10.1007/978-94-017-8539-6_5.
- [21] M. Dular, B. Stoffel, B. Sirok, Development of a cavitation erosion model, *Wear* 261 (5–6) (2006) pp, <https://doi.org/10.1016/j.wear.2006.01.020>.
- [22] C.D. Ohl, S.W. Ohl, ShockWave interaction with single bubbles and bubble clouds, *Bubble Dyn. Shock Waves* (Jan. 2013) 3–31, https://doi.org/10.1007/978-3-642-34297-4_1/COVER.
- [23] J.P. Franc, M. Riondet, A. Karimi, G.L. Chahine, Material and velocity effects on cavitation erosion pitting, *Wear* 274–275 (Jan. 2012) 248–259, <https://doi.org/10.1016/J.WEAR.2011.09.006>.
- [24] W.C. Brunton, J.M. Hobbs, A. Laird, Investigation of a cavitating film erosion test, *Wear* 16 (4) (Oct. 1970) 273–285, [https://doi.org/10.1016/0043-1648\(70\)90251-6](https://doi.org/10.1016/0043-1648(70)90251-6).
- [25] K. Endo, T. Okada, M. Nakashima, A Study of Erosion Between Two Parallel Surfaces Oscillating at Close Proximity in Liquids, *J. Lubr. Technol.* 89 (3) (Jul. 1967) 229–236, <https://doi.org/10.1115/1.3616956>.
- [26] K. Kikuchi, F.G. Hammit, Effect of separation distance on cavitation erosion of vibratory and stationary specimens in a vibratory facility, *Wear* 102 (3) (Apr. 1985) 211–225, [https://doi.org/10.1016/0043-1648\(85\)90219-4](https://doi.org/10.1016/0043-1648(85)90219-4).
- [27] H. Dursun, G. Sevilgen, M.Ý. Karamangil, Experimental investigation of the cavitation erosion of a flat aluminum part using a sonotrode test device, *Materiali in Tehnologije* 53 (5) (2019) 637–642, <https://doi.org/10.17222/MIT.2018.255>.
- [28] I. Hansson, K.A. Mørch, The dynamics of cavity clusters in ultrasonic (vibratory) cavitation erosion, *J. Appl. Phys.* 51 (9) (Sep. 1980) 4651–4658, <https://doi.org/10.1063/1.328335>.
- [29] F. Schreiner, S. Hanke, R. Skoda, Assessment of flow aggressiveness and erosion damage topography for different gap widths in ultrasonic cavitation testing, *Wear* 484–485 (Nov. 2021) 203989, <https://doi.org/10.1016/J.WEAR.2021.203989>.
- [30] A. Priyadarshi, et al., Effect of water temperature and induced acoustic pressure on cavitation erosion behaviour of aluminium alloys, *Tribol. Int.* 189 (2023) 108994, <https://doi.org/10.1016/j.triboint.2023.108994>.
- [31] Y. Gao, M. Zhou, W. Xu, J. Luo, L. Bai, High-speed imaging of supersaturated cavitation clouds and the vibration modes of the radiation surface of high-power transducers, *Ultrason. Sonochem.* 104 (Mar. 2024) 106837, <https://doi.org/10.1016/J.ULTSONCH.2024.106837>.
- [32] G.G.A. Fatjó, A. Torres Pérez, M. Hadfield, Experimental study and analytical model of the cavitation ring region with small diameter ultrasonic horn, *Ultrason. Sonochem.* 18 (1) (Jan. 2011) 73–79, <https://doi.org/10.1016/J.ULTSONCH.2009.12.006>.
- [33] M. Khavari, A. Priyadarshi, A. Hurrell, K. Pericleous, D. Eskin, I. Tzanakis, Characterization of shock waves in power ultrasound, *J. Fluid Mech.* 915 (2021), <https://doi.org/10.1017/jfm.2021.186>.
- [34] L. Bai, P. Wu, H. Liu, J. Yan, C. Su, C. Li, Rod-shaped cavitation bubble structure in ultrasonic field, *Ultrason. Sonochem.* 44 (Jun. 2018) 184–195, <https://doi.org/10.1016/J.ULTSONCH.2018.02.030>.
- [35] L. Bai, J. Yan, Z. Zeng, Y. Ma, Cavitation in thin liquid layer: A review, *Ultrason. Sonochem.* 66 (Sep. 2020) 105092, <https://doi.org/10.1016/J.ULTSONCH.2020.105092>.
- [36] M. Khavari, A. Priyadarshi, A. Hurrell, K. Pericleous, D. Eskin, I. Tzanakis, Characterization of shock waves in power ultrasound, *J. Fluid Mech.* 915 (2021) R3, <https://doi.org/10.1017/JFM.2021.186>.
- [37] A. Žnidarčič, R. Mettin, M. Dular, Modeling cavitation in a rapidly changing pressure field - Application to a small ultrasonic horn, *Ultrason. Sonochem.* 22 (2015), <https://doi.org/10.1016/j.ultrasonch.2014.05.011>.
- [38] A. Žnidarčič, R. Mettin, C. Cairós, M. Dular, Attached cavitation at a small diameter ultrasonic horn tip, *Phys. Fluids* 26 (2) (Feb. 2014) 023304, <https://doi.org/10.1063/1.4866270>.
- [39] L. Yusuf, M. D. Symes, and P. Prentice, "Characterising the cavitation activity generated by an ultrasonic horn at varying tip-vibration amplitudes," 2020, <https://doi.org/10.1016/j.ultrasonch.2020.105273>.
- [40] M. Dular, T. Pozar, J. Zevnik, R. Petkovšek, High speed observation of damage created by a collapse of a single cavitation bubble, *Wear* 418–419 (2019), <https://doi.org/10.1016/j.wear.2018.11.004>.
- [41] M. Dular, C.D. Ohl, Bulk material influence on the aggressiveness of cavitation – Questioning the microjet impact influence and suggesting a possible way to erosion mitigation, *Wear* 530–531 (Oct. 2023) 205061, <https://doi.org/10.1016/J.WEAR.2023.205061>.
- [42] J. Rapet, P.A. Quinto-Su, C.D. Ohl, Cavitation inception from transverse waves in a thin liquid gap, *Phys. Rev. Appl.* 14 (2) (Aug. 2020) 024041, <https://doi.org/10.1103/PHYSREVAPPLIED.14.024041/FIGURES/12/MEDIUM>.
- [43] S. Mottyll, R. Skoda, Numerical 3D flow simulation of ultrasonic horns with attached cavitation structures and assessment of flow aggressiveness and cavitation erosion sensitive wall zones, *Ultrason. Sonochem.* 31 (Jul. 2016) 570–589, <https://doi.org/10.1016/J.ULTSONCH.2016.01.025>.
- [44] F. Reuter, J. Mur, J. Petelin, R. Petkovšek, C.D. Ohl, Shockwave velocimetry using wave-based image processing to measure anisotropic shock emission, *Phys. Fluids* 36 (1) (Jan. 2024) 17127, <https://doi.org/10.1063/5.0180418/3052880>.
- [45] C.E. Brennen, *Cavitation and bubble dynamics*, Oxford University Press, 1995.
- [46] P.A. Quinto-Su, K.Y. Lim, C.D. Ohl, Cavitation bubble dynamics in microfluidic gaps of variable height, *Phys. Rev. E Stat Nonlin Soft Matter Phys* 80 (4) (Oct. 2009) 047301, <https://doi.org/10.1103/PHYSREVE.80.047301/FIGURES/4/MEDIUM>.